QGP parameter extraction via a global analysis of event-by-event flow coefficient distributions

Jonah Bernhard
(Dated: December 13, 2013)

I. INTRODUCTION

Heavy-ion collisions produce a hot, dense phase of strongly-interacting matter known as the quark-gluon plasma (QGP) which quickly ($\sim 10^{-23}$ s) expands and freezes into discrete particles. The QGP cannot be observed directly—only final-state particles are detectable—so computer models are used to indirectly characterize the medium. A successful model must simulate realistic collision events and match its final state to experiment.

Modern models use a "hybrid" approach with relativistic fluid dynamics for the early hot and dense phase followed by non-equilibrium transport for the later dilute gas phase. Hybrid models have provided approximate descriptions of a variety of observables, but are very computationally expensive and therefore difficult to test systematically, so they remain poorly constrained.

One of the most important properties of the QGP is its shear viscosity to entropy density ratio η/s. The QGP is postulated to behave as a near-ideal fluid, hence its viscosity may be nearly minimal. This is explored primarily via collective flow measurements—a natural partner, since viscosity tends to damp collective behavior. Previous studies have tentatively confirmed a small η/s, typically by matching event-averaged flow between model and experiment.

The ATLAS experiment has recently measured event-by-event flow distributions, which could provide a much more sensitive probe of η/s. We systematically test a hybrid model by calculating flow distributions over wide ranges of η/s and other salient model parameters and calibrating to ATLAS data. This model-to-data comparison will provide optimal values of each parameter—some of which are physical properties of the QGP—and clarify the important features of a physically accurate model.

II. RELATIVISTIC HEAVY-ION COLLISIONS

In normal matter, quarks and gluons are confined to composite particles known as hadrons by the strong nuclear force. The theory which describes these interactions, quantum chromodynamics (QCD), predicts a fluid-like phase of deconfined quarks and gluons at sufficiently high temperature and density. This QCD phase is commonly called the quark-gluon plasma (QGP).

It is postulated that the universe was one large QGP in the first microseconds after the Big Bang, before freezing into hadrons. Similar conditions can be created—on a much smaller scale—in high-energy nuclear collisions. Simple models of the QGP in such collisions were proposed forty years ago [1].

The timescale of relativistic heavy-ion collisions is extremely short, order 10^{-23} seconds, and the created matter is correspondingly small, order 10^{-15} meters (1 fm). Therefore collisions cannot be resolved in time or space; all that can be observed are the final-state particles which stream into the detector.

Experiments are ongoing at the Relativistic Heavy-Ion Collider (RHIC) at Brookhaven National Lab and the Large Hadron Collider (LHC) at the European Organization for Nuclear Research. RHIC collides copper, gold, and uranium nuclei at center of mass energies up to 200 GeV per nucleon-nucleon pair. The LHC program performs lead-lead collisions at 2.76 TeV.

A. Spacetime evolution

The dynamics of relativistic boost-invariant nuclear collisions were semi-quantitatively described by Bjorken in 1983 [3]. Figure 1 shows a schematic of the spacetime evolution. In the center of mass frame, nuclei approach each other at (nearly) the speed of light, Lorentz-contracted into almost-flat discs. They collide at time $t = 0$, depositing energy and creating new matter in the process. This new matter is presumably not initially in thermal equilibrium. The system has thermalized by time $t \sim 1$ fm/c after the collision, while the discs recede at the speed of light. The thermal material (QGP) expands and cools until $t \sim 10$ fm/c, when it freezes into hadrons.

If one views the collision in a somewhat boosted frame ($\gamma \lesssim 3$), it still looks like a pair of Lorentz-contracted discs colliding and receding. This implies approximate boost invariance near mid-rapidity, where spacetime rapidity is defined as

$$\eta_s = \frac{1}{2} \ln \frac{t+z}{t-z}. \tag{1}$$

The central rapidity region ($|\eta_s| \lesssim 3$) contains the hot, dense, fluid-like medium, and most particle production occurs in central rapidity. The partner variable to spacetime rapidity is the proper time

$$\tau^2 = t^2 - z^2, \tag{2}$$

which defines hyperbolic surfaces on which the fluid is approximately uniform.

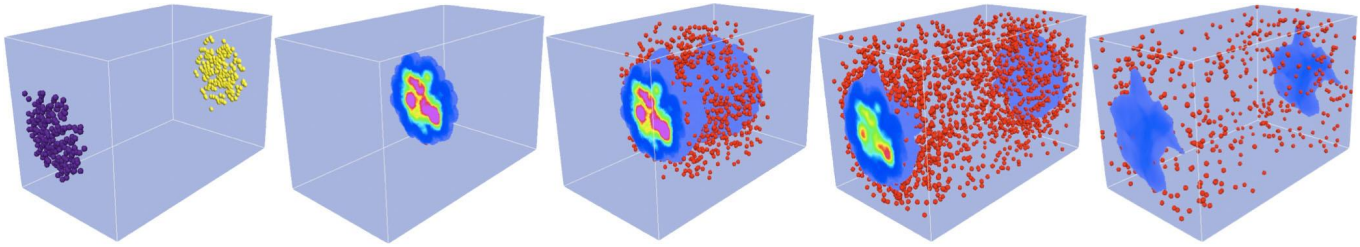

FIG. 1. Schematic evolution of a relativistic heavy-ion collision. The points in the left frame represent nucleons in colliding nuclei. The colored volumes represent QGP, and the red points are hadrons produced in QGP freeze-out. Figure from [2].

B. Collective behavior and flow

The QGP is a strongly-interacting fluid-like phase with a very short mean free path, and is therefore expected to exhibit collective behavior, i.e. emitted particles are correlated in phase space.

Ollitrault showed that anisotropies in transverse momentum distributions are an unambiguous signal of transverse collective flow [4]. Consider a peripheral collision of two disc-like nuclei where the impact parameter is large enough that the overlap region is an asymmetrical almond shape, as in Fig. 2. This creates a larger pressure gradient along the direction of the impact parameter—the reaction plane. This causes the system to expand more quickly in the reaction plane, converting the initial-state spatial anisotropy into final-state momentum anisotropy.

The efficiency of this position-to-momentum space conversion depends primarily on the shear viscosity of the fluid. A small shear viscosity corresponds to a strongly-interacting system with a small mean free path; a large viscosity means strong dissipative effects and damped collective behavior. The effect of viscosity is demonstrated in Fig. 4. QGP viscosity is conventionally expressed as a dimensionless ratio of the shear viscosity to the entropy density, η/s.

Anisotropic flow is parameterized by decomposing the transverse-momentum distribution into its Fourier components:

$$\frac{dN}{d\phi} = \frac{N}{2\pi}\left\{1 + \sum_n v_n \cos[n(\phi - \Psi)]\right\}, \tag{3}$$

where ϕ is the azimuthal angle of transverse momentum, Ψ is the reaction-plane angle, and the v_n are the flow coefficients. Each v_n describes the magnitude of the nth-order momentum anisotropy: v_2 corresponds to elliptic flow, v_3 to triangular flow, etc., as in Fig. 3.

The observation of collective flow provides essential evidence for the existence of a strongly-interacting QCD phase. Such behavior is a general property of strongly-interacting systems, ranging from the QGP to an ultracold degenerate Fermi gas [5].

C. Fluctuations

The circular nuclei depicted in Fig. 2 represent an average over many events. In this average scenario, the elliptic flow v_2 dominates due to asymmetric overlap, but higher-order even coefficients (v_4, v_6, ...) are much smaller and all odd-order flows (v_3, v_5, ...) vanish.

More realistic collisions have randomly distributed nucleons and irregular overlap regions, e.g. as in Fig. 4. These initial-state fluctuations mean that *all* flow coefficients are in general nonzero on an event-by-event level. v_2 will typically be the largest coefficient for a peripheral collision, since it is driven by systematic initial-state anisotropy, while v_3, v_4, etc. are driven by fluctuations alone. In a central collision, i.e. one with zero impact parameter and maximal overlap, all flows including v_2 are caused solely by fluctuations.

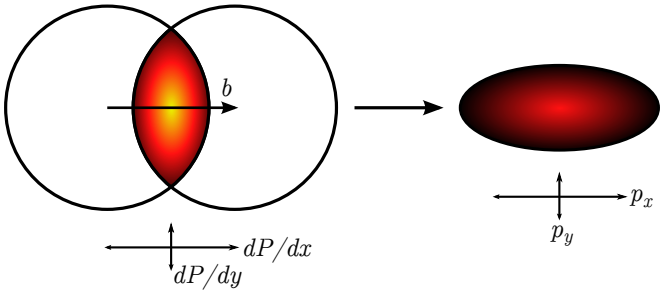

FIG. 2. Development of elliptic flow in a peripheral collision. The asymmetric overlap region creates a pressure gradient anisotropy $dP/dx > dP/dy$, which drives fluid flow in the x-direction.

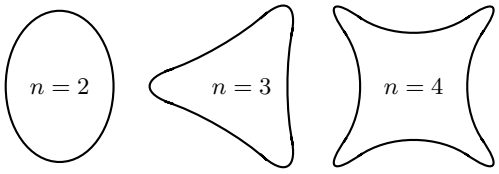

FIG. 3. Fourier components of flow.

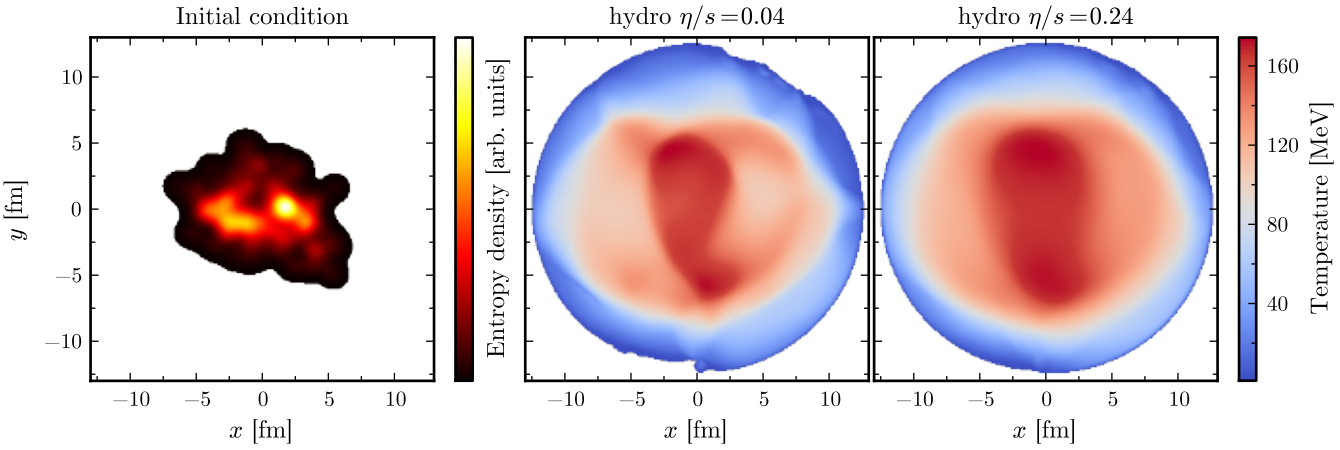

FIG. 4. Left: Initial condition from the MC-Glauber model for a Pb-Pb collision at 2.76 TeV and $b = 8$ fm. The initial condition is then evolved with viscous hydro. Middle: The hydro medium at $\tau = 8$ fm/c with viscosity $\eta/s = 0.04$. Right: $\eta/s = 0.24$.

Measurement of event-by-event flows provides flow probability distributions $P(v_n)$. The mean, width, and shape of these distributions are important probes of QGP properties, notably the viscosity η/s.

III. SIMULATIONS

Modern heavy-ion collision simulations employ Monte Carlo (MC) models for the initial state, viscous relativistic fluid dynamics for the hot and dense stage, and non-equilibrium Boltzmann transport for the late dilute hadron gas phase [6–8].

A. Initial conditions

An event is initialized by a randomly generated energy or entropy density profile. The MC-Glauber model [9] is the simplest: it first randomly samples nucleon positions, then calculates energy or entropy density in the plane transverse to the beam based on the overlap between colliding nucleons. The Glauber model produces energy density from both binary collisions (direct interactions between pairs of nucleons) and wounded nucleons (any participating nucleon). A parameter α sets the wounded nucleon / binary collision mixture as $\frac{1}{2}(1-\alpha)\mathrm{WN}+\alpha\,\mathrm{BC}$. Figure 4 shows a sample initial condition generated by the Glauber model.

The MC-KLN model [10] samples nucleon positions (as in Glauber) and calculates the nucleon densities in each nucleus. The local saturation scale Q_s is determined and used to calculate the gluon distribution functions. The resulting gluon density is then proportional to energy density. The energy and momentum dependence of Q_s is set by a parameter λ.

B. Relativistic hydrodynamics

A hydrodynamics code takes the initial condition input and evolves it until freeze-out. Typically, the pre-equilibrium phase is ignored, and the initial condition is simply expanded without any interactions until some initial time $\tau_0 \sim 1$ fm/c.

At time τ_0, the medium is assumed to have thermalized, and hydro evolution begins. Hydro codes solve the conservation equations

$$\partial_\mu T^{\mu\nu} = 0, \tag{4}$$

where

$$T^{\mu\nu} = (\epsilon + P)u^\mu u^\nu - P g^{\mu\nu} + \pi^{\mu\nu} \tag{5}$$

is the stress-energy tensor. ϵ, P, and u^μ are the energy density, pressure, and flow velocity of the fluid, $g^{\mu\nu}$ is the metric tensor, and $\pi^{\mu\nu}$ is the shear stress tensor which accounts for dissipation due to viscosity η/s. When viscosity is included, the shear relaxation time τ_Π naturally enters the equations.

An equation of state,

$$P = P(\epsilon), \tag{6}$$

is also required and usually provided by lattice QCD, e.g. s95-PCE [11].

Some hydro codes reduce computational complexity by assuming boost-invariance at mid-rapidity and explicitly calculating only the transverse directions. "Time" is actually the proper time τ, i.e. the medium is calculated on proper-time hyperbola. Such codes are called 2+1D, meaning two spatial dimensions and time. Figure 4 shows an example 2+1D hydro calculation.

C. Hadronic freeze-out

Hydro evolution stops when a pre-specified criterion is satisfied, typically when the temperature has cooled to the QCD transition at $T \sim 165$ MeV. The medium then freezes into discrete hadrons on a spacetime hypersurface σ with spectra given by the Cooper-Frye formula [12]

$$E\frac{dN_i}{d^3p} = \int_\sigma f_i(x,p)\, p^\mu\, d^3\sigma_\mu, \tag{7}$$

where f_i is the particle distribution function, p^μ is the four-momentum, and $d^3\sigma_\mu$ is an infinitesimal piece of the hypersurface σ whose magnitude is the volume of the element and direction is normal to the element. The subscript i is an index over particle species.

The Cooper-Frye formula may be integrated directly to yield spectra. In a hybrid model, it is randomly sampled to produce an ensemble of particles.

D. Transport

The particle ensemble is given to a hadronic transport code such as Ultrarelativistic Quantum Molecular Dynamics (UrQMD) [13, 14]. The transport algorithm calculates collisions and decays by solving the Boltzmann equation

$$\frac{df_i(x,p)}{dt} = \mathcal{C}_i(x,p), \tag{8}$$

where f_i is the particle distribution function, $\mathcal{C}_i$ is the collision kernel which describes source terms, and i is an index over species. The results from the transport code are analogous to particles which stream into a detector.

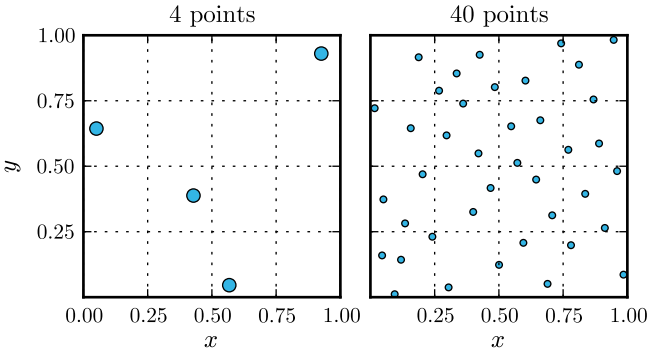

FIG. 5. Left: four points from a Latin-hypercube sample in two variables x, y. Grid lines are drawn to guide the eye; only one point is present in each row and column. Right: LHS of 40 points (20 per dimension).

IV. METHOD

A. Model-to-data comparison

A generic model-to-data comparison consists of a computer model which requires a set of input parameters and a corresponding set of experimental data. The input parameters must be calibrated so that the model optimally reproduces reality.

If the model runs quickly, simple techniques such as Markov chain Monte Carlo (MCMC) may be used. However, this requires many (10^6) evaluations of the model and hence is not feasible for slower codes.

Heavy-ion collision models are very computationally expensive: each event requires roughly an hour of CPU time, and at least 10^3 events are required for a statistically significant study of event-by-event fluctuations. Input parameters correlate with each other and affect multiple observables, so it is not sufficient to calibrate each parameter independently—all must be varied simultaneously.

A pair of strategies help reduce the required amount of CPU time:

- Evaluate the model at a predetermined set of parameter points.
- Interpolate between explicitly calculated points.

Suppose a certain model has M input parameters which must be calibrated to data. The simplest set of parameter points is a factorial design: select N evenly-spaced values for each parameter and evaluate the model at all possible combinations. However, this requires N^M parameter points which grows very rapidly, e.g. 5 parameters with 10 values each needs 10^5 total points. This scheme is also prone to wasted CPU time, since unlikely parameter values will be evaluated many times.

A much more efficient design is achieved via Latin-hypercube sampling (LHS). LHS is ideal for slowly-

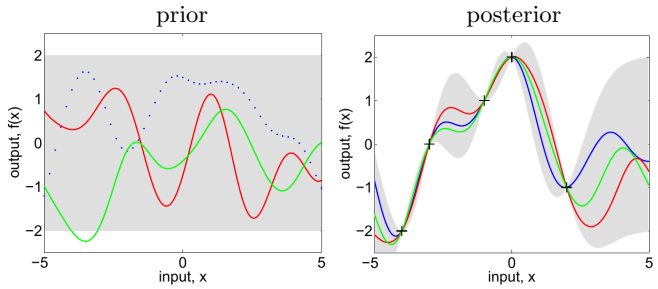

FIG. 6. Left: three random functions drawn from a Gaussian process prior. One is plotted as a series of points, the others have the points connected into a curve. Right: three random functions drawn from the posterior, i.e. the prior conditioned on the observations indicated by plus signs. The shaded band represents 2σ error bands; notice how the posterior error is small near the observed points and large further away. Figures from [15].

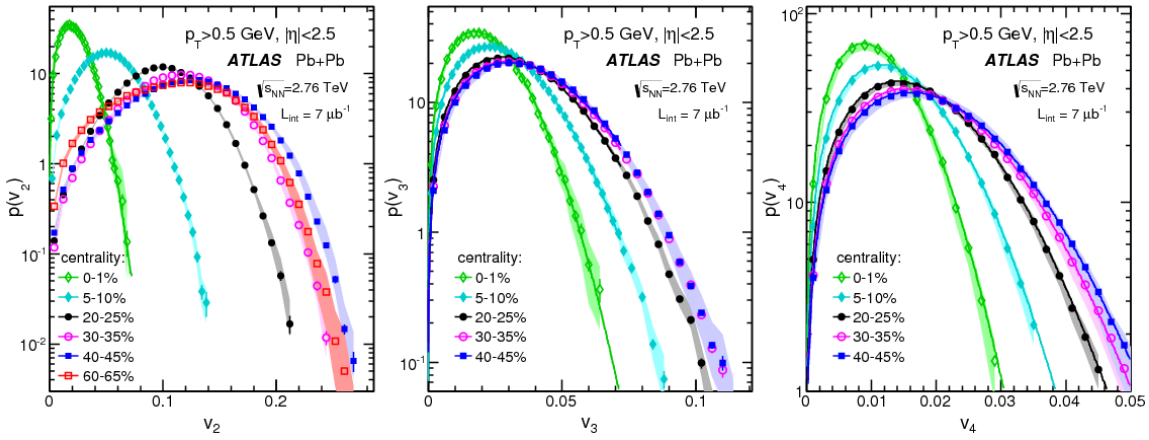

FIG. 7. ATLAS event-by-event flow distributions for v_2 (left), v_3 (middle), and v_4 (right) for several centrality bins. Error bars are statistical errors, bands are systematic uncertainties on the distribution shape, lines are fits to the Rice distribution Eq. (13). Figure from [16].

varying models, i.e. one which produces similar results for nearby points in parameter space. A LHS provides randomly sampled parameter points subject to some conditions:

- The *minimum* distance between points is *maximized*.
- Parameter values are not repeated.

This way, the parameter space is optimally filled without wasting CPU time calculating redundant information. A typical choice for a Latin-hypercube design is 20 points per dimension, see e.g. Fig. 5.

Sparse designs may be interpolated by a Gaussian process emulator [15]. A Gaussian process (GP) is generalization of a Gaussian distribution: instead of drawing random values from a distribution, random functions are drawn from a process. Gaussian processes require a covariance function, e.g. the covariance of a one-dimensional GP between two points x_1, x_2 could be

$$\mathrm{cov}(x_1, x_2) \propto \exp\left[-\frac{(x_1 - x_2)^2}{\ell^2}\right] \tag{9}$$

where ℓ is the correlation length, so that nearby points are strongly correlated and distant points are independent.

When used for interpolation, a GP emulator assumes that the model is a generic GP (the prior) and is trained on the Latin-hypercube points to produce conditioned GPs (the posterior). The posterior provides a statistical distribution of the model outputs with more certainty closer to explicitly calculated points, hence, it acts as a fast surrogate to the actual model while reflecting the true state of knowledge. Figure 6 shows a generic one-dimensional example.

B. Experimental data

The ATLAS experiment at the LHC has measured event-by-event flow probability distributions for v_2, v_3, v_4 from Pb-Pb collisions at 2.76 TeV [16, 17].

Flows are calculated event-by-event as two-dimensional vectors $\vec{v}_n = (v_{n,x}, v_{n,y})$ using the single-particle definition

$$v_{n,x} = \langle \cos n\phi \rangle, \quad v_{n,y} = \langle \sin n\phi \rangle, \tag{10}$$

where the average is over all particles in the event. The flow coefficients are the vector magnitudes

$$v_n = |\vec{v}_n| = \sqrt{v_{n,x}^2 + v_{n,y}^2}. \tag{11}$$

The probability distribution of flow vectors is assumed to follow a bivariate Gaussian

$$P(\vec{v}_n) = \frac{1}{2\pi\delta_{v_n}^2} e^{-\frac{(\vec{v}_n - \vec{v}_n^{\,\mathrm{RP}})^2}{2\delta_{v_n}^2}}, \tag{12}$$

where $\vec{v}_n^{\,\mathrm{RP}}$ is the average flow vector and δ_{v_n} is the width of fluctuations around the mean. The one-dimensional distribution of magnitudes is obtained by integrating out the azimuthal angle in Eq. (12) and is called the Rice or Bessel-Gaussian distribution:

$$P(v_n) = \frac{v_n}{\delta_{v_n}^2} e^{-\frac{(v_n)^2 + (v_n^{\mathrm{RP}})^2}{2\delta_{v_n}^2}} I_0\left(\frac{v_n^{\mathrm{RP}} v_n}{\delta_{v_n}^2}\right), \tag{13}$$

where I_0 is the modified Bessel function of the first kind. ATLAS fits their data to the Rice distribution, thereby reducing each distribution to two parameters, v_n^{RP} and δ_{v_n}. The Gaussian assumption is excellent for central collisions and acceptable for peripheral collisions, where the tails fall off somewhat more sharply than a Gaussian.

Observed flow distributions are smeared by finite-multiplicity fluctuations and physical nonflow effects such

as jets. The true distribution $P(v_n)$ will result in an observed distribution [18]

$$P(v_n^{\rm obs}) = \int P(v_n^{\rm obs}|v_n)P(v_n)\,dv_n, \qquad (14)$$

where the response function $P(v_n^{\rm obs}|v_n)$ gives the probability of observing flow $v_n^{\rm obs}$ from an event with true flow v_n. ATLAS determines the true flow distribution by measuring the response function directly from the data and iteratively solving Eq. (14) with a Bayesian unfolding procedure [19].

C. Computer experiment design

Simulated event-by-event flow distributions are calculated with a modern hybrid model using MC-Glauber [9] and MC-KLN [10] initial conditions, viscous 2+1D hydrodynamics [20], a Cooper-Frye hypersurface sampler [2], and UrQMD [13, 14]. It is an updated version of the OSU/Duke model VISHNU (Viscous Hydro and UrQMD) [8].

A set of the five most salient model parameters is selected for calibration. The initial condition normalization must be calibrated, though it is not a physical parameter, since it sets the total amount of entropy deposited in a collision. For the Glauber model, the wounded nucleon / binary collision parameter α is varied; for KLN, the saturation scale exponent λ is chosen. The variable hydro parameters are the thermalization time τ_0, specific shear viscosity η/s, and shear relaxation time τ_Π. Table I summarizes the parameters.

Parameter points are generated from a 256-point five-dimensional Latin hypercube. The initial goal is 1000 events per design point, in the centrality bins 0–5%, 5–10%, ..., 50–55%, and both Glauber and KLN models, for a total of 3 million events. At roughly one hour per event, this represents over 300 years of CPU time. Events are run in parallel on the Open Science Grid (OSG), which can execute 10^4 events simultaneously and provide 10^5 CPU hours per day.

The event-by-event model and all utilities for running on the OSG are publicly available at `https://github.com/jbernhard/ebe-osg`. This package automates running batches of events on the OSG with easy tuning of input parameters. Results are copied directly from OSG machines to storage space at Duke.

Parameter	Glauber	KLN
Normalization	20–60	5–15
α	0.05–0.30	—
λ	—	0.1–0.3
τ_0	0.2–1.0 fm/c	
η/s	0.0–0.3	
τ_Π	0.2–1.1 fm/c	

TABLE I. Input parameter ranges for calibration.

D. Data analysis

Observed flows are calculated from UrQMD output using the same single-particle method as ATLAS; $v_n^{\rm RP}$ and δ_{v_n} are then extracted via a maximum-likelihood fit to the Rice distribution. Finite-multiplicity smearing still must be removed, but unlike the experimental distributions, the "detector" is perfectly efficient and nonflow effects are absent. The response function results from pure Gaussian statistical smearing, hence it is another Rice distribution:

$$P(v_n^{\rm obs}|v_n) = \frac{v_n^{\rm obs}}{\delta_{v_n}^2} e^{-\frac{(v_n^{\rm obs})^2+(v_n)^2}{2\delta_{v_n}^2}} I_0\left(\frac{v_n v_n^{\rm obs}}{\delta_{v_n}^2}\right) \qquad (15)$$

where the width depends only on the multiplicity M as [4, 16, 18]

$$\delta_{v_n}^2 = 1/2M. \qquad (16)$$

Since both the true flow distribution and the statistical smearing are Gaussian, the observed distribution will be yet another Rice distribution:

$$P(v_n^{\rm obs}) = \frac{v_n^{\rm obs}}{(\delta_{v_n}^{\rm obs})^2} e^{-\frac{(v_n^{\rm obs})^2+(v_n^{\rm RP})^2}{(\delta_{v_n}^{\rm obs})^2}} I_0\left(\frac{v_n^{\rm RP} v_n^{\rm obs}}{(\delta_{v_n}^{\rm obs})^2}\right) \qquad (17)$$

where $v_n^{\rm RP}$ is unaffected by the smearing but the width is increased as

$$(\delta_{v_n}^{\rm obs})^2 = \delta_{v_n}^2 + 1/2M. \qquad (18)$$

Hence, finite-multiplicity effects may be removed by reducing the value of δ_{v_n} from the maximum-likelihood fit according to the multiplicity.

The code used to analyze all model output is publicly available at `https://github.com/jbernhard/ebe-analysis`, though it is still a work in progress.

V. RESULTS

The initial batch of OSG events is complete, with 1000–2000 events for each combination of parameter point, centrality class, and initial condition model, for a total of 3.5 million events. Assuming a Pb-Pb cross section of 7.65 barn, this equates to an integrated luminosity of $\sim 0.5\ \mu{\rm b}^{-1}$ (ATLAS results are based on $7\ \mu{\rm b}^{-1}$).

All flow distributions are calculated and $v_n^{\rm RP}, \delta_{v_n}$ are extracted. The average flow $\langle v_n\rangle$, width σ_{v_n}, and relative fluctuation $\sigma_{v_n}/\langle v_n\rangle$ are also calculated. The emulator is not yet in use.

Figure 8 shows model output using Glauber initial conditions for v_2 in the 20-25% centrality bin. Flow distribution parameters are plotted against each of the five variable model parameters. Note that all input parameters vary simultaneously due to the Latin-hypercube design, so the horizontal axes have implicitly flattened the variation of all other parameters. Most of the apparent noise

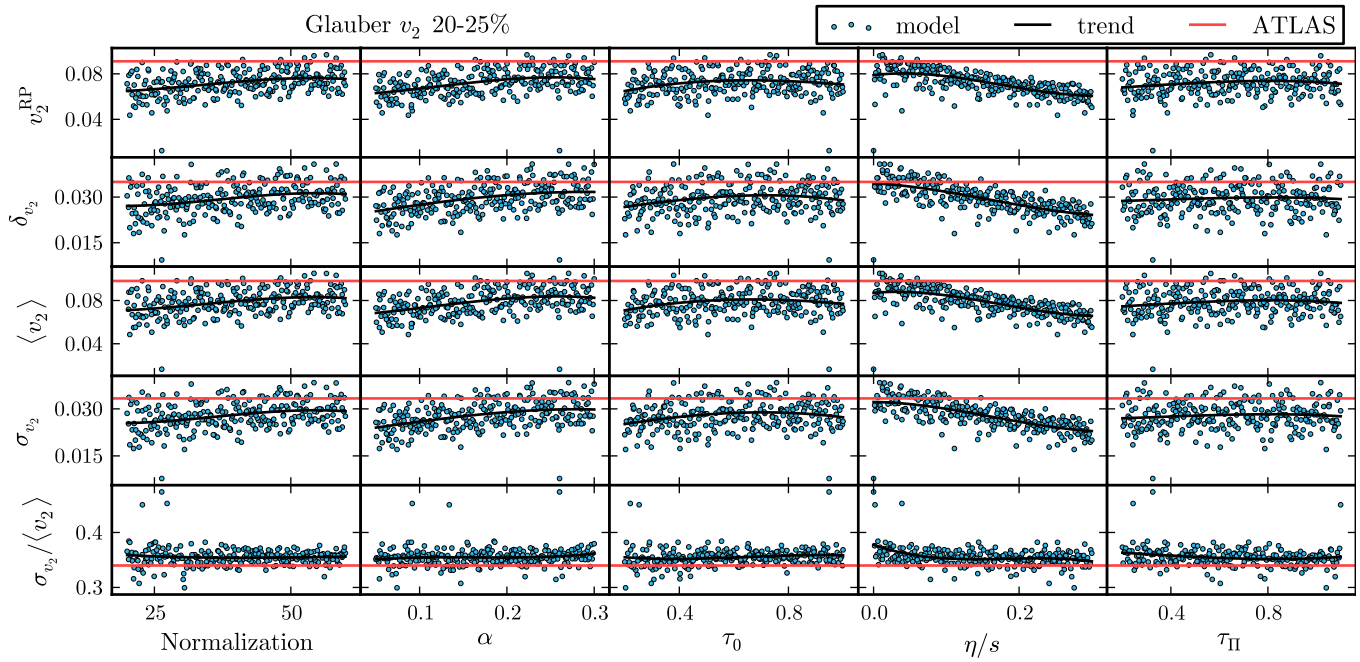

FIG. 8. Dependence of flow distribution parameters on model parameters for v_2 in the 20–25% centrality bin using the Glauber initial condition model. Scatterplots are model output, black lines are trendlines to guide the eye, and red lines denote the experimental ATLAS values.

can be attributed to other parameters changing. Eventually, the emulator will allow varying a single parameter while keeping all others fixed.

The viscosity η/s appears to be the single most influential parameter. In particular, flow tends to decrease as η/s increases. Other parameters show somewhat weaker correlations, except for τ_Π which appears to have no effect.

At this time, goodness of fit is quantified by comparing average flow $\langle v_n \rangle$ between model and experiment. The average flows from the best Latin-hypercube points are plotted in Fig. 9. The input parameters for the best Glauber point are

$$\alpha = 0.27,\ \tau_0 = 0.46\ \mathrm{fm/c},\ \eta/s = 0.026,\ \tau_\Pi = 1.0\ \mathrm{fm/c};$$

the best point for KLN is

$$\lambda = 0.25,\ \tau_0 = 0.70\ \mathrm{fm/c},\ \eta/s = 0.21,\ \tau_\Pi = 0.28\ \mathrm{fm/c}.$$

These are *not* the best-fit parameters from the model, they are the values corresponding to the Latin-hypercube point whose average flows best match ATLAS.

Figure 10 shows the preferred η/s as a function of centrality. Again, the values come directly from Latin-hypercube points and do not represent actual best fits. For the Glauber model, the preferred values for noncentral v_2 and v_3 are quite consistent; the most central bin (0–5%) and all v_4 show more noise. This is expected: Glauber is too rudimentary to accurately capture small-scale initial-state fluctuations, so it has little hope of accurately predicting fluctuation-only flows. It performs best with noncentral v_2, where flow is driven by systematic initial-state anisotropy. The KLN model prefers a larger η/s than Glauber for v_2, but is not self-consistent across all v_n, notably underpredicting v_3.

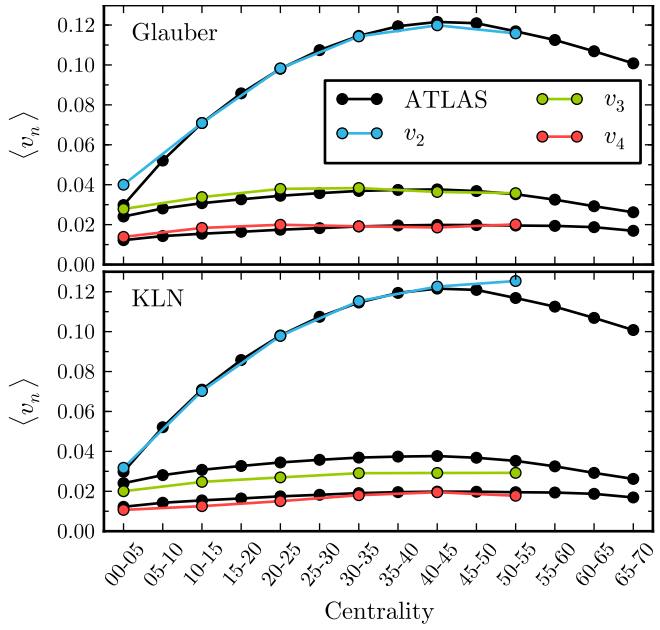

FIG. 9. Average v_2 (blue), v_3 (green), and v_4 (red) compared to ATLAS values (black). Top: Best Glauber Latin-hypercube point. Bottom: Best KLN point.

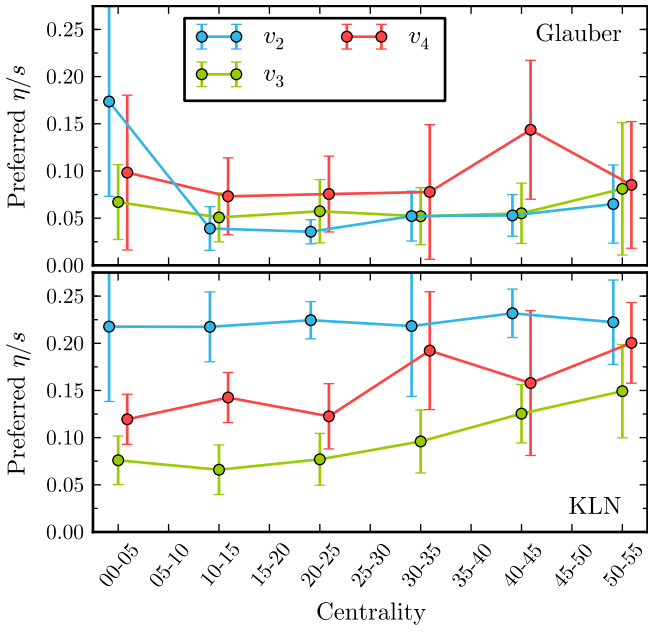

FIG. 10. Preferred η/s as a function of centrality. Data points are the average η/s from the best 10 Latin-hypercube points by average v_n, error bars are the standard deviation of the best 10. Top: Glauber model. Bottom: KLN.

These preliminary results are consistent with previous studies using similar models [8, 21, 22].

VI. CONCLUSION

An event-by-event relativistic heavy-ion collision model is systematically tested on a massive scale. The model is calibrated to event-by-event flow distributions from the ATLAS experiment. Preliminary results agree with previous work.

Several important tasks remain: Goodness of fit must be quantified more rigorously and include all flow distribution parameters. Other observables should be considered, for example the charged-particle multiplicity. A Gaussian process emulator will provide a continuous and intuitive picture of the parameter space.

A large portion of this project is developing a framework for calibrating computationally expensive event-by-event models to data. Now that the framework is in place, the analysis can quickly be repeated for other models. Future plans include upgrading the initial conditions to a more realistic model and hydro code to a full 3+1D algorithm.

[1] G. Chapline, M. Johnson, E. Teller, and M. Weiss, Phys.Rev. **D8**, 4302 (1973).
[2] Z. Qiu, (2013), arXiv:1308.2182 [nucl-th].
[3] J. Bjorken, Phys.Rev. **D27**, 140 (1983).
[4] J.-Y. Ollitrault, Phys.Rev. **D46**, 229 (1992).
[5] K. O'Hara, S. Hemmer, M. Gehm, S. Granade, and J. Thomas, Science **298**, 2179 (2002), arXiv:cond-mat/0212463 [cond-mat.supr-con].
[6] S. Bass and A. Dumitru, Phys.Rev. **C61**, 064909 (2000), arXiv:nucl-th/0001033 [nucl-th].
[7] C. Nonaka and S. A. Bass, Phys.Rev. **C75**, 014902 (2007), arXiv:nucl-th/0607018 [nucl-th].
[8] H. Song, S. A. Bass, U. Heinz, T. Hirano, and C. Shen, Phys.Rev.Lett. **106**, 192301 (2011), arXiv:1011.2783 [nucl-th].
[9] M. L. Miller, K. Reygers, S. J. Sanders, and P. Steinberg, Ann.Rev.Nucl.Part.Sci. **57**, 205 (2007), arXiv:nucl-ex/0701025 [nucl-ex].
[10] H.-J. Drescher, A. Dumitru, A. Hayashigaki, and Y. Nara, Phys.Rev. **C74**, 044905 (2006), arXiv:nucl-th/0605012 [nucl-th].
[11] P. Huovinen and P. Petreczky, Nucl.Phys. **A837**, 26 (2010), arXiv:0912.2541 [hep-ph].
[12] F. Cooper and G. Frye, Phys.Rev. **D10**, 186 (1974).
[13] S. Bass, M. Belkacem, M. Bleicher, M. Brandstetter, L. Bravina, *et al.*, Prog.Part.Nucl.Phys. **41**, 255 (1998), arXiv:nucl-th/9803035 [nucl-th].
[14] M. Bleicher, E. Zabrodin, C. Spieles, S. Bass, C. Ernst, *et al.*, J.Phys. **G25**, 1859 (1999), arXiv:hep-ph/9909407 [hep-ph].
[15] C. E. Rasmussen and C. K. I. Williams, *Gaussian Processes for Machine Learning* (The MIT Press, 2006).
[16] G. Aad *et al.* (ATLAS Collaboration), (2013), arXiv:1305.2942 [hep-ex].
[17] J. Jia (ATLAS Collaboration), (2012), arXiv:1209.4232 [nucl-ex].
[18] B. Alver *et al.* (PHOBOS Collaboration), Phys.Rev.Lett. **104**, 142301 (2010), arXiv:nucl-ex/0702036 [nucl-ex].
[19] J. Jia and S. Mohapatra, (2013), arXiv:1304.1471 [nucl-ex].
[20] H. Song and U. W. Heinz, Phys.Rev. **C77**, 064901 (2008), arXiv:0712.3715 [nucl-th].
[21] C. Shen, S. A. Bass, T. Hirano, P. Huovinen, Z. Qiu, *et al.*, J.Phys. **G38**, 124045 (2011), arXiv:1106.6350 [nucl-th].
[22] U. Heinz, C. Shen, and H.-C. Song, AIP Conf.Proc. **1441**, 766 (2012), arXiv:1108.5323 [nucl-th].